Arch Appl Mech (2010) 80: 161–173
DOI 10.1007/s00419-009-0307-0

ORIGINAL

C. M. Sands · H. W. Chandler · I. A. Guz · Y. A. Zhuk

Extending the Bodner–Partom model to simulate the response of materials with extreme kinematic hardening

Received: 14 November 2008 / Accepted: 30 January 2009 / Published online: 20 February 2009
© Springer-Verlag 2009

Abstract This paper demonstrates that, at extreme levels of kinematic hardening, the traditional formulation of the Bodner–Partom model can produce anomalous results. The reasons for this anomalous behaviour are explained, and a reformulated version of the model is presented. This reformulation extends the range of the model to include levels of kinematic hardening that may be problematic in the traditional formulation. The formulation of the model is adjusted so as to retain the rate dependency of the original Bodner–Partom model; and to permit the values of the material parameters used with the traditional formulation to be re-used with the extended model—with the exception only of the hardening coefficients which become dimensionless constants holding different numerical values. This revised formulation also imposes associated flow, thereby ensuring phase consistency between stress and plastic strain during non-proportional loading. In this way, the anomalies are removed, the range and stability of the model is increased, and all the advantages and important features of the Bodner–Partom model are retained.

Keywords Viscoplastic · Creep · Nonlinear · Modelling · Plasticity

1 Introduction

The Bodner–Partom model is a viscoplastic model with creep originally designed to simulate the behaviour of metals that undergo creep at high temperatures. It is a mature model, originally created in 1975 [1] with only isotropic work hardening. It has undergone a number of subsequent modifications to incorporate kinematic hardening, recovery and the changing response of the material to variations in temperature [2], and continues to be used [3–11].

Formally, the Bodner–Partom model does not require an explicit yield surface and so can reproduce the experimentally observed smooth transition from low level creep deformation to high strain-rate plasticity as the loads are increased. However, with appropriate choices of the values of constants, it can successfully

Supported by EPSRC: EP/E30351/1.

C. M. Sands (✉) · I. A. Guz
Centre for Micro- and Nanomechanics, School of Engineering, University of Aberdeen,
Aberdeen AB24 3UE, Scotland, UK
E-mail: c.sands@abdn.ac.uk
Tel.: +44-1224 27-2499
Fax: +44-1224 27-2497

H. W. Chandler
School of Engineering, University of Aberdeen, Aberdeen AB24 3UE, Scotland, UK

Y. A. Zhuk
Timoshenko Institute of Mechanics, 3, Nesterov Street, 03057 Kiev, Ukraine

approximate a sharp yield point, as shown in the work of Esat et al. [12]. This flexibility gives obvious benefits to the modelling of a wide range of materials. In fact, recently, researchers have exploited the benefits of the Bodner–Partom model to simulate the mechanical response of certain non-metallic materials whose behaviour phenomenologically resembles that of metal creep [13–15], while other researchers [16] have acknowledged this facility. Additionally, as the Bodner–Partom model has no fixed yield point, it could be used to simulate plasticity at small strains.

It has been recognised [17], however, that the Bodner–Partom model (as currently formulated) may present erroneous predictions when used to simulate non-proportional loading and when operating at low strain rates. Work presented in the current paper demonstrates that issues also exist if kinematic hardening is extreme. There is no suggestion, however, that the model does not provide perfectly acceptable predictions when used for the range of behaviour for which it was originally intended, simply that issues may exist when departing from proven capability.

While many other viscoplastic models exist (an excellent review [17] has recently been published), the Bodner–Partom model remains popular and has been widely used for more than 30 years—indicating a significant investment of time and effort by many researchers. It is, therefore, timely to examine the features of the Bodner–Partom model that can give rise to anomalous or erroneous behaviour and propose alterations to the formulation that address these issues while permitting researchers to utilise the wealth of knowledge gained from past experience with this model. This paper describes a number of changes which would allow a more extended range of stress–strain behaviour to be simulated with the Bodner–Partom model and that the authors incorporated into an existing computer program with relative ease.

This paper starts by reviewing the development of the Bodner–Partom model and the results of some simulations are presented. The significance of these results, some of which are anomalous, are discussed, stressing the limitations they indicate. Particular attention is paid to the case of cyclic loading where kinematic hardening is extreme. In that case, during unloading, secondary inelastic deformation occurs before the unloading is complete. This exposes some deep-seated issues with the implementation of kinematic hardening in the Bodner–Partom model. Finally, a reformulated version of the model is presented that may have advantages when the extent of kinematic hardening is problematic in the existing formulation, and when non-proportional loading is being simulated.

2 Preliminaries

Consider an elastic–viscoplastic body lying in a Cartesian coordinate system with coordinates x_1, x_2 and x_3. Components of the infinitesimal strain tensor are denoted by ε_{ij}. The components ($\dot{e}_{ij}$) of the deviatoric part of the strain rate tensor are defined as

$$\dot{e}_{ij} = \dot{\varepsilon}_{ij} - \dot{\varepsilon}_{mm}\delta_{ij}/3, \tag{1}$$

where δ_{ij} represents the Kronecker delta. A dot over a symbol indicates a time derivative, or rate, and Einstein's summation convention has been used throughout this paper. The components of the deviatoric strain rate consist of elastic ($\dot{e}^E_{ij}$) and inelastic ($\dot{e}^I_{ij}$) contributions such that

$$\dot{e}_{ij} = \dot{e}^E_{ij} + \dot{e}^I_{ij}. \tag{2}$$

The components of the stress tensor are denoted by σ_{ij} and the components (s_{ij}) of the deviatoric part are given by

$$s_{ij} = \sigma_{ij} - \sigma_{mm}\delta_{ij}/3. \tag{3}$$

The elastic components of the volumetric strain ε^E_{mm}, and the deviatoric strain e^E_{ij} are related to the mean stress ($\sigma_{mm}/3$) and components of deviatoric stress through Hooke's law in the usual way

$$\varepsilon^E_{mm} = \frac{\sigma_{mm}}{3K} \tag{4}$$

$$e^E_{ij} = \frac{s_{ij}}{2G}, \tag{5}$$

where K and G are the bulk and shear moduli, respectively.

Consistent with these definitions, the rate of inelastic dissipation ($\dot{W}^I$) is given by

$$\dot{W}^I = s_{ij}\dot{e}^I_{ij}, \tag{6}$$

assuming that the hidden energy of cold work is negligible.

3 Formulation of Bodner–Partom models

The isothermal version of the Bodner–Partom model, without kinematic hardening, can be presented as relying on three assumptions:

1. The magnitude of the plastic strain rate is given by

$$\sqrt{\dot{e}^I_{ij}\dot{e}^I_{ij}} = \sqrt{2.0D_0^2 \exp\left(-\left(\frac{(Z^I)^2}{3J_2}\right)^n\right)}, \tag{7}$$

   where J_2 is the second invariant of the deviatoric stress tensor ($s_{ij}s_{ij}/2$); Z^I represents the material resistance to inelastic flow at the current material state; and the model constants are defined in Table 1.
2. The inelastic contribution is incompressible and obeys the Prandtl–Reuss equations

$$\dot{e}^I_{ij} = \lambda s_{ij}, \tag{8}$$

   where λ is a plastic multiplier and is given by $\sqrt{\dot{e}^I_{ij}\dot{e}^I_{ij}}/\sqrt{s_{rs}s_{rs}}$.
3. The evolution of Z^I is given by the differential equation

$$\dot{Z}^I = m_1(Z_1 - Z^I)\dot{W}^I - A_1 Z_1\left(\frac{Z^I - Z_2}{Z_1}\right)^{r_1}, \tag{9}$$

   with the first term representing the saturation of hardness and the second term representing the recovery.

The incorporation of kinematic hardening introduces a tensor with components of stress β_{ij} which evolves according to the differential equation

$$\dot{\beta}_{ij} = m_2(Z_3 u_{ij} - \beta_{ij})\dot{W}^I - A_2 Z_1\left(\frac{\sqrt{\beta_{rs}\beta_{rs}}}{Z_1}\right)^{r_2}\left(\frac{\beta_{ij}}{\sqrt{\beta_{rs}\beta_{rs}}}\right), \tag{10}$$

Table 1 Interpretation of model parameters

Parameters	Description
G (MPa)	Shear modulus
K (MPa)	Bulk modulus
m_1 (MPa^{-1})	Coefficient for isotropic hardening
m_2 (MPa^{-1})	Coefficient for kinematic hardening
A_1 (s^{-1})	Recovery rate coefficient for isotropic hardening
A_2 (s^{-1})	Recovery rate coefficient for kinematic hardening
D_0 (s^{-1})	Limiting (maximum) strain rate
Z_0 (MPa)	Initial value for isotropic hardening
Z_1 (MPa)	Limiting (maximum) value for isotropic hardening
Z_2 (MPa)	Fully recovered (minimum) value for isotropic hardening
Z_3 (MPa)	Limiting (maximum) value for kinematic hardening
n	Strain rate sensitivity parameter
r_1	Recovery exponent for isotropic hardening
r_2	Recovery exponent for kinematic hardening

where u_{ij} are the components of a tensor defined as

$$u_{ij} = \frac{s_{ij}}{\sqrt{s_{rs}s_{rs}}}. \tag{11}$$

This is then used to form

$$Z^D = \beta_{ij}u_{ij}, \tag{12}$$

a scalar contribution to the resistance to inelastic flow, modifying assumption (1) to give

$$\sqrt{\dot{e}^I_{ij}\dot{e}^I_{ij}} = \sqrt{2.0D_0^2 \exp\left(-\left(\frac{(Z^I + Z^D)^2}{3J_2}\right)^n\right)}. \tag{13}$$

This approach can be used to give quite realistic models of the stress–strain response varying with time at a specific temperature, as shown in Fig. 1 and by [18–21]. It is, however, relatively easy to pick parameters that do not lead to sensible stress–strain curves, especially if cyclic deformation is demanded. An example is shown in Fig. 2. It may be argued that careful choice of the values of the parameters would avoid this type of behaviour. However, in order to simulate the cyclic behaviour of polymers or granular materials, extreme levels of kinematic hardening are needed and this leads inevitably to severe problems with the traditional formulation of the Bodner–Partom model containing kinematic hardening and recovery—hereafter referred to simply as the Bodner–Partom Model (BPM).

4 Simulations

A number of simulations were performed to illustrate features of the model. An implicit algorithm for the Bodner–Partom model was developed using an optimization procedure to solve the system of non-linear equations at each increment of strain. A number of simulations were run and the results obtained checked using another

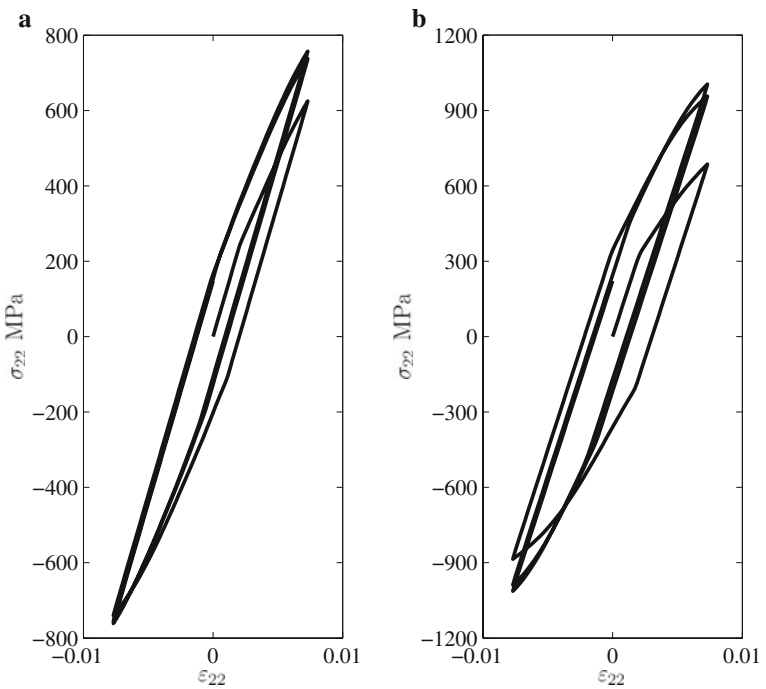

Fig. 1 Stress–strain curves for three loading cycles at a strain rate of 0.015 s^{-1}, with the material properties 1 (**a**), and material properties 3 (**b**) shown in Table 2

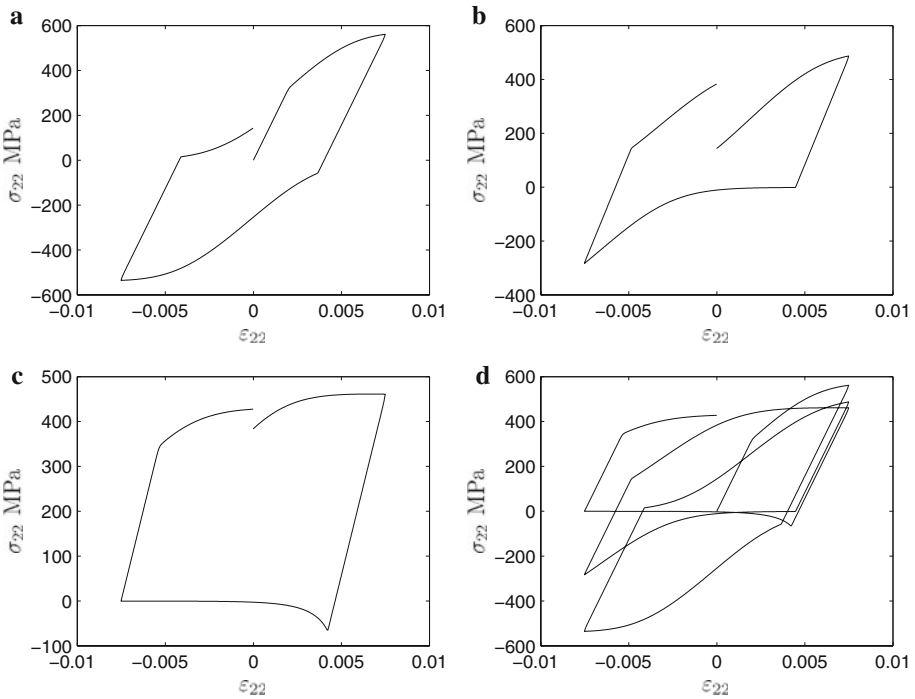

Fig. 2 Stress–strain curves for three loading cycles at a strain rate of 0.015 s^{-1} with the material properties 2 given in Table 2; showing the first cycle (**a**), the second cycle (**b**), the third cycle (**c**) and all three cycles (**d**)

Table 2 Parameters for tensile test simulations

	Parameters 1	Parameters 2	Parameters 3
G	44,000	61,500	61,500
K	123,000	133,000	133,000
m_1	0.09	0.002	0.1
m_2	2.5	1.5	1.5
A_1	0.2	0.15	0.15
A_2	0.5	0.05	0.05
D_0	10000.0	10000.0	10000.0
Z_0	500.0	1000.0	1000.0
Z_1	2000.0	2000.0	3500.0
Z_2	200.0	200.0	1000.0
Z_3	800.0	800.0	800.0
n	2.5	1.5	1.5
r_1	0.9	0.9	0.9
r_2	0.2	0.5	0.9

Units given in Table 1

algorithm [22–24] and published results [1]. A cyclic tensile test was then simulated, with the strain increasing to a maximum and then reversing for three cycles, using a variety of material parameters listed in Table 2. Care was taken to ensure that convergence was achieved at every increment and no evidence of non-uniqueness was found.

Figures 1 and 2 clearly show that broadly similar material parameters can give radically different results and those shown in Fig. 2 are clearly highly suspect.

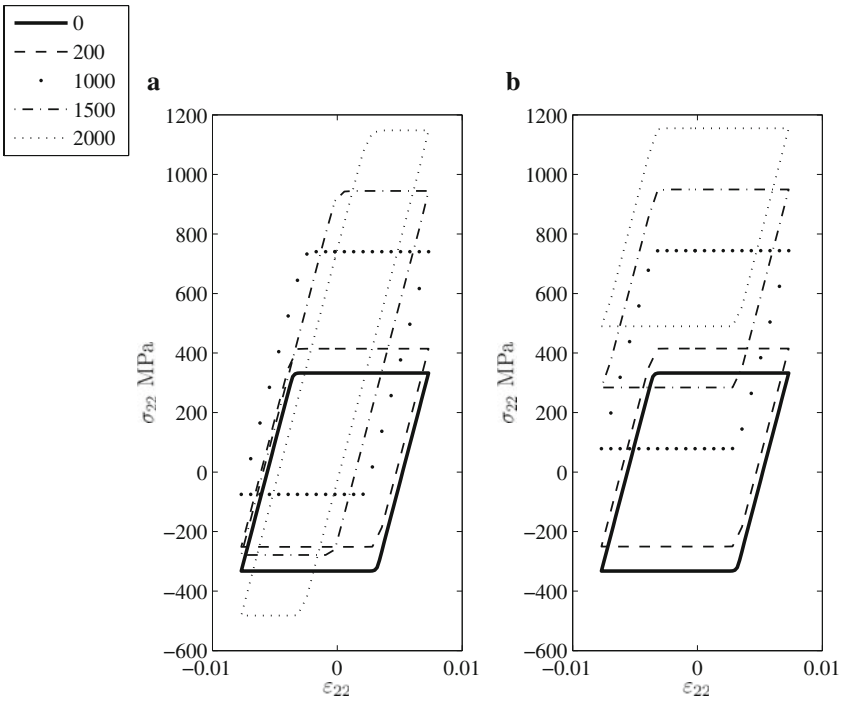

Fig. 3 Stress–strain curves for levels of fixed kinematic hardness shown, at a strain rate of 0.015 s^{-1}, with the material properties shown in Table 3 using BPM (**a**) and PEM (**b**)

5 Exploring the anomalous behaviour

Detailed inspection of the results indicates that these problems first manifest themselves when the kinematic hardening is sufficiently severe that on unloading Z^D is both negative and comparable in magnitude to Z^I. The simulations become pathological if their sum becomes negative. Of course the original model was never designed to simulate such an extreme case, however the usefulness of the overall approach is such that extension into these ranges would be useful, not only for particular materials but also when using automatic means of determining the best choice of parameters to reproduce experimental data.

In understanding this feature of the model it may be helpful to start by examining how the kinematic hardening, as defined within the traditional formulation, effects the behaviour of the model. Figure 3a shows a series of steady state cyclic loading curves for a fixed strain rate of 0.015 s^{-1} (simulated by incrementing e_{22}) and using identical material parameters (given in Table 3) but with the kinematic hardening set to different values by altering the values of β_{ij} at the start of the simulation. Values of β_{22} of 0.0, 200.0, 1000.0, 1500.0 and 2000.0 MPa were chosen with the other diagonal components being equal and chosen to maintain $\beta_{mm} = 0$. With values of β_{22} from zero to 1000 MPa, the stress–strain loop shifts as anticipated. The maximum stress reached increases with increasing β_{22}, but the difference between the maximum and minimum stress remains constant. The horizontal shift in the stress–strain loops is caused by the elastic shift from the start tensile stress of 300 MPa. The increase in kinematic hardness from 1500.0 to 2000.0 MPa, however, manifests an anomalous increase in the difference between the maximum and minimum stress.

Specifically, in the traditional formulation of the Bodner–Partom model the ratio $(Z^I)^2/J_2$ can be thought of as the resistance to flow divided by a measure of the stress producing the flow. Kinematic hardening is incorporated by modifying the resistance to flow to $(Z^D + Z^I)^2$. This works well for moderate amounts of kinematic hardening. If, however, one needs to have sufficiently severe kinematic hardening that $Z^D + Z^I$ becomes negative during strain reversal then the above formulation will produce these spurious results.

An alternative way to incorporate kinematic hardening is to let the resistance remain unaltered, but instead modify the stress invariant. This has been the approach utilized by [25] and [26] through the incorporation of a back stress tensor with components ρ_{ij} to give J_2^K defined by

$$J_2^K = (s_{ij} - \rho_{ij})(s_{ij} - \rho_{ij})/2. \tag{14}$$

Table 3 Parameters for plots in Fig. 3

	Parameters
G	61,500
K	133,000
m_1	0.0
m_2	0.0
A_1	0.0
A_2	0.0
D_0	10,000
Z_0	1,000
Z_1	3,500
Z_2	1,000
Z_3	800.0
n	1.5
r_1	0.9
r_2	0.9

Units given in Table 1

Equation 13 could be reformulated as

$$\sqrt{\dot{e}^I_{ij}\dot{e}^I_{ij}} = \sqrt{2.0D_0^2 \exp\left(-\left(\frac{(Z^I)^2}{3J_2^K}\right)^n\right)}, \tag{15}$$

with $\rho_{ij} = \beta_{ij}$. However, the sensitivity to deformation rate would be changed. The original sensitivity can be preserved, and the original parameter values reused, if $\rho_{ij} = F\beta_{ij}$ where

$$F = \sqrt{2/3}\left(-2\ln(\sqrt{\dot{e}_{ij}\dot{e}_{ij}}/D_0)\right)^{-1/2n}. \tag{16}$$

Running simulations with this modification exposed problems with the use of the Prandtl–Reuss equations when $\dot{d}_{22}$ and s_{22} were required to have opposite signs. The solution was to use the associated flow rule where

$$\dot{e}^I_{ij} = \lambda(s_{ij} - \rho_{ij}), \tag{17}$$

and λ is a plastic multiplier ($\sqrt{\dot{e}^I_{ij}\dot{e}^I_{ij}}/\sqrt{2J_2^K}$).

These reformulations, together—hereafter referred to as the *Partially Extended Bodner–Partom Model* (PEM)—resolve the anomaly shown in Fig. 3a (as can be seen from Fig. 3b). Figure 4 demonstrates that the PEM retains the original rate dependency of the Bodner–Partom model, permitting the use of the original values of the material constants. The model could, therefore, be used without the factor F in Eq. 16; but it would, essentially, be a different model. A wealth of investigation has demonstrated that the rate dependency of the Bodner–Partom model gives good agreement with experimental results for a range of strain rates. This confidence would be lost if Eq. 16 were omitted from the formulation of the model.

The simulation shown in Fig. 2d (obtained using the traditional formulation of the Bodner–Partom model) is reproduced in Fig. 5a to facilitate comparison with simulations obtained using variations of the partially extended Bodner–Partom model. The simulation shown in Fig. 5b demonstrates the results of extending the model by only incorporating the revised flow rule shown in Eq. 17. Clearly no improvement in the results was achieved. Figure 5c shows the results obtained by only incorporating the revised invariant (J_2^K)—demonstrating that this modification is responsible for removing the anomalous dip in the stress–strain curve shown in Fig. 2c. Only two cycles are shown as convergence was not achieved in the third cycle. This, together with the simulation shown in Fig. 5d (which uses the full PEM incorporating both modifications) demonstrates that these modifications are not sufficient to solve all the problems and the anomaly resulting from the form of the evolution of Z^I and β still has to be addressed.

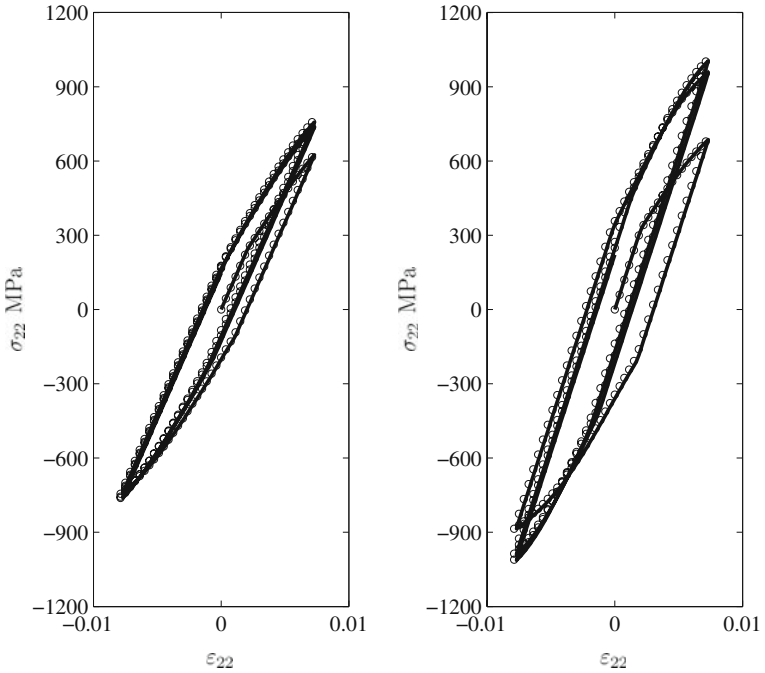

Fig. 4 Reproduction of the simulations shown in Fig. 1 (*solid line*) with simulations using a version of the model (PEM) using Eqs. 14, 15, 16 and 17 (*open circle*)

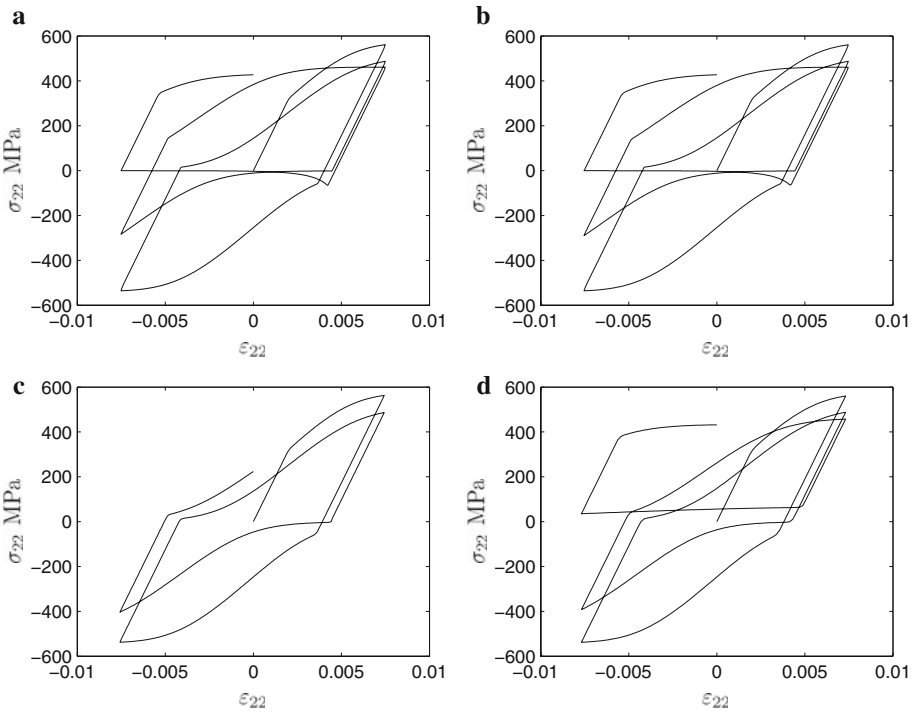

Fig. 5 The simulation illustrated in Fig. 2 using BPM (**a**); reproduced using PEM with Eq. 17 only (**b**); using PEM with J_2^K only (**c**); and using the full PEM (**d**). Table 2 shows the material properties

5.1 Examining the evolution of Z^I and β_{ij}

The treatment of the evolution of the isotropic and kinematic hardening may be approached in a number of ways. While the Bodner–Partom model interprets the description "work hardening" literally and uses the work done as the ongoing variable in the evolution equations, an alternative is to use an equivalent plastic strain instead. The latter approach was used to model non-linear kinematic hardening by Armstrong and Fredericks [26] in the context of rate independent plasticity and extended to viscoplasticity by Malinin and Khadjins [27].

The evolution equations for the isotropic hardening and kinematic hardening state variables, Z^I and β_{ij} (see Eqs. 9 and 10) contain the rate of inelastic work ($\dot{W}^I$). As this is based on stress, it will be zero if the stress is zero (if recovery is ignored). However, the rate of plastic strain could well be large, leading to the anomalous prediction of perfect plasticity and the 'flat' region in the stress strain curves observed in Figs. 2 and 5 at zero stress. One possible way of coping with this would be to use *strain* hardening rather than *work* hardening. Then

$$\dot{Z}^I = m_1' \left(Z_1 - Z^I\right) \sqrt{\dot{e}_{ij}^I \dot{e}_{ij}^I} - A_1 Z_1 \left(\frac{Z^I - Z_2}{Z_1}\right)^{r_1} \tag{18}$$

and

$$Z^D = \beta_{ij} u_{ij}; \tag{19}$$

where

$$\dot{\beta}_{ij} = m_2'(Z_3 \dot{u}_{ij}^I - \beta_{ij}) \sqrt{\dot{e}_{ij}^I \dot{e}_{ij}^I} - A_2 Z_1 \left(\frac{\sqrt{\beta_{rs}\beta_{rs}}}{Z_1}\right)^{r_2} \left(\frac{\beta_{ij}}{\sqrt{\beta_{rs}\beta_{rs}}}\right), \tag{20}$$

and m_1' and m_2' retain the meaning given in Table 1 for m_1 and m_2 respectively, but are now dimensionless constants holding different numerical values. The values of all the other material constants remain unchanged. This model will be referred to as *the extended Bodner–Partom model* (EBP) in the rest of this paper. Values of $m_1' = 50$ and $m_2' = 833$ were used with this extended Bodner–Partom model for the simulation shown (○) in Fig. 6a, and $m_1' = 60$ and $m_2' = 500$ were used for the simulation shown (○) in Fig. 6b.

Using these values as a guide, the simulation shown in Fig. 2 was repeated using the extended Bodner–Partom model with $m_1' = 1.16$ and $m_2' = 500$, retaining the original values of all other material constants. The results are shown in Fig. 7. The simulation shown in Fig. 2 has been reproduced in Fig. 7a, to facilitate comparison with simulations obtained using the extended Bodner–Partom model, which has been run for 3 cycles in Fig. 7b, and for 30 cycles in Fig. 7c to demonstrate the model stability. The simulation for the first cycle using the extended Bodner–Partom model is shown as the thick line in Fig. 7d, superimposed on the results obtained with the Bodner–Partom model (shown as the thin line) to show that the extended Bodner–Partom model produces the same results as the Bodner–Partom model if appropriate values are chosen for m_1' and m_2' (i.e. 1.16 and 500, respectively).

It should be recognized that the material parameters used were deliberately selected so as to expose these features, which may well not manifest themselves when the traditional formulation is used, with appropriate material properties, to simulate metal plasticity and creep. There is, however, no guarantee that these features will not manifest themselves, to a greater or lesser extent, if this formulation is applied to materials whose properties (with regard to this model formulation) fall outside the traditional metal plasticity envelope. Although the features discussed here are illustrated particularly dramatically in Figs. 2 and 3a, they can occur almost unobtrusively, depending on the material parameters, loading configuration and strain rate. It should be remembered that the curves in these figures were obtained after full convergence at every increment and are, therefore, genuine results for the material properties, model formulation and loading used. These features are of considerable significance if a "least squares", or similar optimization routine, is used to establish material parameters from experimental data. Like the traditional formulation, the extended Bodner–Partom model presented in this paper, is restricted to small strains. Sansour and Kollmann [28], however, have proposed a general formulation of elasto-viscoplasticity at large strains and shown how it can be applied to the Bodner–Partom model. Their approach could be applied to the modified formulation presented in this paper. It follows that the researcher should choose the most appropriate formulation of the Bodner–Partom model for their purposes.

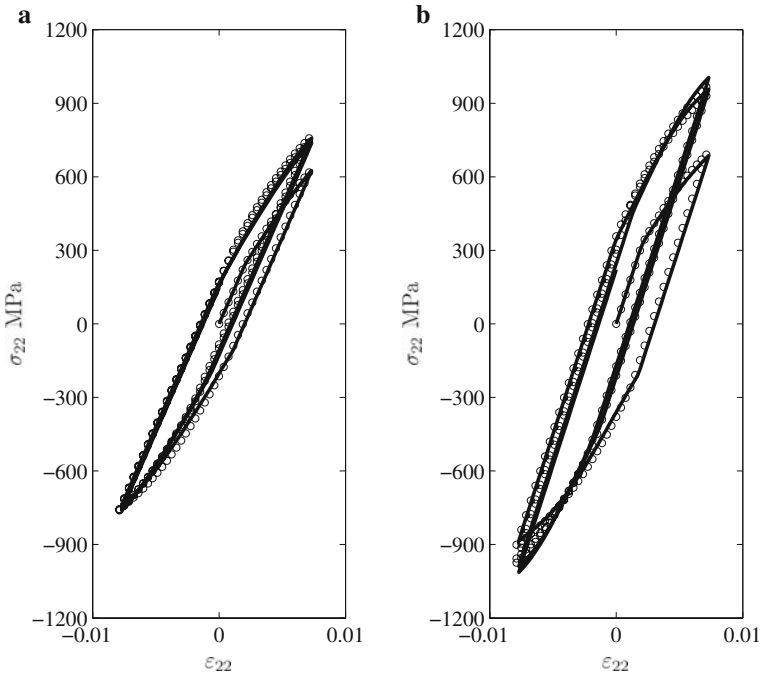

Fig. 6 Reproduction of the simulation shown in Fig. 1 (*solid line*) with a simulation using the extended Bodner–Partom model (EBP) (*open circle*); with $m_1' = 50$, $m_2' = 833$ (**a**) and $m_1' = 60$, $m_2' = 500$ (**b**)

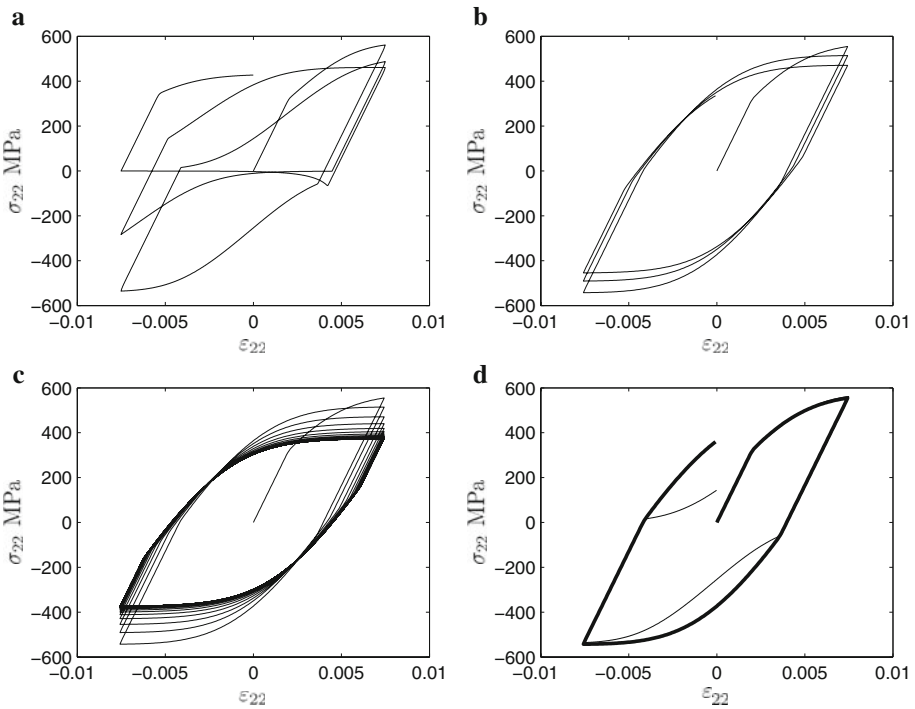

Fig. 7 The simulation shown in Fig. 2 using BPM (**a**); repeated using EBP with $m_1' = 1.16$ and $m_2' = 500$ for three cycles (**b**); for 30 cycles (**c**); and the first cycle using EBP (*thick line*) and BPM (*thin line*) (**d**)

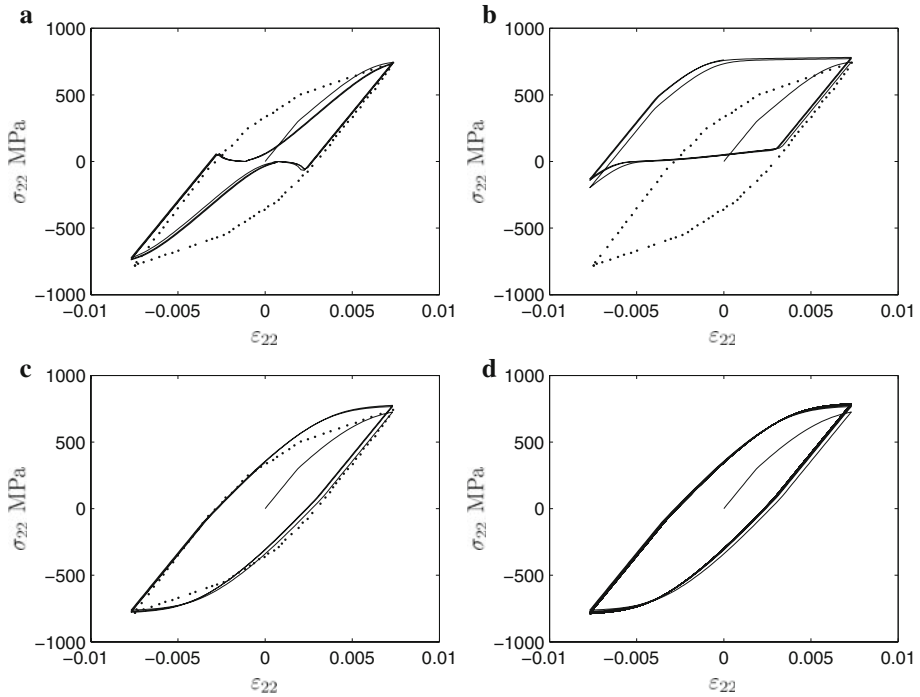

Fig. 8 Re-presentation of a simulation (*dotted line*) from [29] with those (*solid line*) obtained using the different versions of the Bodner–Partom model presented in this paper—see text for details

Table 4 Parameters for plots in Fig. 8

	Parameters
G	61,500
K	133,000
m_1	0.00151
m_2	2.61
A_1	0.152
A_2	0.0527
D_0	10,000
Z_0	565
Z_1	3,987
Z_2	565
Z_3	818.0
n	2.72
r_1	0.875
r_2	0.157

Units given in Table 1

6 Comparison with experimental data

The three versions of the Bodner–Partom model explored in this paper were used to simulate experimental results published by Andersson et al. [29] and the results are shown in Figure 8. Andersson's results are indicated by a dotted line and those obtained using the the versions of the Bodner–Partom model explored in this paper are indicated by a solid line. The traditional formulation of the Bodner–Partom model is shown in Fig. 8a, the partially extended Bodner–Partom model is shown in Fig. 8b and the extended Bodner–Partom model is shown in Fig. 8c—all for three cycles. Figure 8d shows the extended Bodner–Partom model running for 30 cycles to demonstrate the stability of the fully extended version of the model. The values

used for the model constants are shown in Table 4, with $m'_1 = 0.876$ and $m'_2 = 870$ in the extended version.

Andersson used a formulation of the Bodner–Partom model that reduced the number of non-linear equations and increased the speed of convergence by using two different formulations based on the value of λ [30]. The model constants used in the simulations presented here have been chosen to mimic those used by Andersson; showing the ease with which the extended Bodner–Partom model can be applied to existing data.

7 Conclusions

1. This paper has demonstrated that previous formulations of the Bodner–Partom model can produce pathological results when kinematic hardening is sufficiently extreme that $Z^I + Z^D$ becomes negative.
2. This paper has demonstrated that, at high levels of kinematic hardening, the use of work hardening rather than strain hardening is inappropriate.
3. A modification to the flow rule avoids these problems while retaining the strain rate dependency of the original formulation and only requiring the values of two of the model's fourteen parameters to be adjusted.
4. The proposed modifications should entail only minimal alteration to existing computer code and will maintain the relevance of data obtained with the original formulation.

References

1. Bodner, S.R., Partom, Y.: Constitutive equations for elastic–viscoplastic strain-hardening materials. J. Appl. Mech. Trans. ASME **42**(2), 385–389 (1975)
2. Bodner, S.R.: Unified plasticity—an engineering approach. Tech. rep., Faculty of Mechanical Engineering, Technion, Israel Institute of Technology, Israel (2000)
3. Cecot, W.: Adaptive FEM analysis of selected elastic–viscoplastic problems. Comput. Methods Appl. Mech. Eng. **196**(37–40), 3859–3870 (2007)
4. Andersson, H.: An implicit formulation of the Bodner–Partom constitutive equations. Comput. Struct. **81**(13), 1405–1414 (2003)
5. Foringer, M.A., Robertson, D.D., Mall, S.: A micromechanistic-based approach to fatigue life modeling of titanium–matrix composites. Compos. Part B Eng. **28**(5–6), 507–521 (1997)
6. Klosowski, P., Woznica, K., Weichert, D.: Comparison of numerical modelling and experiments for the dynamic response of circular elasto-viscoplastic plates. Eur. J. Mech. Solids **19**(2), 343–359 (2000)
7. Liang, R.Q., Khan, A.S.: A critical review of experimental results and constitutive models for BCC and FCC metals over a wide range of strain rates and temperatures. Int. J. Plast. **15**(9), 963–980 (1999)
8. Shi, J., Liu, C.R.: The influence of material models on finite element simulation of machining. J. Manuf. Sci. Eng. Trans. ASME **126**(4), 849–857 (2004)
9. Zhuk, Y.A., Senchenkov, I.K., Kozlov, V.I., Tabieva, G.A.: Axisymmetric dynamic problem of coupled thermovisoplasticity. Int. Appl. Mech. **37**(10), 1311–1317 (2001)
10. Rowley, M.A., Thornton, E.A.: Constitutive modeling of the visco-plastic response of Hastelloy-X and aluminium alloy 8009. J. Eng. Mater. Technol. Trans. ASME **118**(1), 19–27 (1996)
11. Zhuk, Y.A., Guz, I.A.: Active damping of forced vibration of hinge-ended beam containing piezoactive layers with account of geometrical and physical nonlinearity. Int. Appl. Mech. (2009, in press)
12. Esat, I.I., Bahai, H., Shati, F.K.: Finite element modelling of anisotropic elastic–viscoplastic behaviour of metals. Finite Elem. Anal. Des. **32**(4), 279–287 (1999)
13. Rubin, M.B., Bodner, S.R.: A three-dimensional nonlinear model for dissipative response of soft tissue. Int. J. Solids Struct. **39**(19), 5081–5099 (2002)
14. Mazza, E., Papes, O., Rubin, M.B., Bodner, S.R., Binur, N.S.: Nonlinear elastic–viscoplastic constitutive equations for aging facial tissues. Biomech. Model. Mechanobiol. **4**(2–3), 178–189 (2005)
15. Pyrz, M., Zairi, F.: Identification of viscoplastic parameters of phenomenological constitutive equations for polymers by deterministic and evolutionary approach. Model. Simul. Mater. Sci. Eng. **15**(2), 85–103 (2007)
16. Chaboche, J.L.: Thermodynamic formulation of constitutive equations and application to the viscoplasticity and viscoelasticity of metals and polymers. Int. J. Solids Struct. **34**(18), 2239–2254 (1997)
17. Chaboche, J.L.: A review of some plasticity and viscoplasticity constitutive theories. Int. J. Plast. **24**(10), 1642–1693 (2008)
18. Chan, K.S., Bodner, S.R., Walker, K.P., Lindholm, U.S.: A survey of unified constitutive theories. In: Proceedings of the Second Symposium on Nonlinear Constitutive Relationships for High Temperature Applications, pp. 1–23. Cleveland, Ohio (1984)
19. Chan, K.S., Lindholm, U.S., Bodner, S.R., Walker, K.P.: High temperature inelastic deformation under uniaxial loading: theory and experiment. J. Eng. Mater. Technol. Trans. ASME **111**, 345–353 (1989)
20. Chan, K.S., Lindholm, U.S., Bodner, S.R., Nagy, A.: High temperature inelastic deformation of the B1900+Hf alloy under multiaxial loading: theory and experiment. J. Eng. Mater. Technol. Trans. ASME **112**(1), 7–14 (1990)
21. Chan, K.S., Lindholm, U.S.: Inelastic deformation under nonisothermal loading. J. Eng. Mater. Technol. Trans. ASME. **112**(1), 15–25 (1990)

22. Zhuk, Y.A., Senchenkov, I.K.: Resonance vibrations and dissipative heating of thin-walled laminated elements made of physically nonlinear materials. Int. Appl. Mech. **40**(7), 794–802 (2004)
23. Zhuk, Y.A., Chervinko, O.P., Tabieva, G.A.: Planar flexural vibrations and dissipative heating of laminated rectangular plates. Int. Appl. Mech. **38**(7), 837–844 (2002)
24. Zhuk, Y.A., Senchenkov, I.K., Tabieva, G.A., Chervinko, O.P.: Axisymmetric vibrations and dissipative heating of a laminated inelastic disc. Int. Appl. Mech. **38**(1), 95–102 (2002)
25. Lemaitre, J., Chaboche, J.L.: Mechanics of Solid Materials. Cambridge University Press, Cambridge (1990)
26. Armstrong, P.J., Fredericks, C.O.: A mathematical representation of the multiaxial Bauschinger effect. Tech. rep., CEGB report No. RD/B/N 731 (1966)
27. Malinin, N.N., Khadjins, G.M.: Theory of creep with anisotropic hardening. Int. J. Mech. Sci. **14**(4), 235 (1972)
28. Sansour, C., Kollmann, F.G.: On theory and numerics of large viscoplastic deformation. Comput. Methods Appl. Mech. Eng. **146**(3–4), 351–369 (1997)
29. Andersson, H., Persson, C., Hansson, T., Melin, S., Järvstråt, N.: Constitutive dependence in finite-element modelling of crack closure during fatigue. Fatigue Fract. Eng. Mater. Struct. **27**(2), 75–87 (2004)
30. Andersson, H.: Personal communication